ADVANCED FUNCTIONAL MATERIALS
www.afm-journal.d

One-Step Scalable Fabrication of Graphene-Integrated Micro-Supercapacitors with Remarkable Flexibility and Exceptional Performance Uniformity

Xiaoyu Shi, Feng Zhou, Jiaxi Peng, Ren'an Wu, Zhong-Shuai Wu, and Xinhe Bao*

The rapid development of miniature electronics has accelerated the demand for simplified and scalable production of micro-supercapacitors (MSCs); however, the preparation of active materials, patterning microelectrodes, and subsequent modular integration of the reported MSCs are normally separated and are involved in multiple complex steps. Herein, a one-step, cost-effective strategy for fast and scalable fabrication of patterned laser-induced graphene (LIG) for all-solid-state planar integrated MSCs (LIG-MSCs) with various form factors of designable shape, exceptional flexibility, performance uniformity, superior modularization, and high-temperature stability is demonstrated. Notably, using the conductive and porous LIG patterns composed of randomly stacked graphene nanosheets simultaneously acting as both microelectrodes and interconnects, the resulting LIG-MSCs represent typical electrical double capacitive behavior, having an impressive areal capacitance of 0.62 mF cm^{-2} and long-term stability without capacitance degeneration after 10 000 cycles. Furthermore, LIG-MSCs display exceptional mechanical flexibility and adjustable voltage and capacitance output through arbitrary arrangement of cells connected in series and in parallel, indicative of exceptional performance customization. Moreover, all-solid-state LIG-MSCs working at ionogel electrolyte exhibit highly stable performance even at high temperature of 100 °C, with 90% capacitance retention over 3000 cycles, suggestive of outstanding reliability. Therefore, the LIG-MSCs offer tremendous opportunities for miniature power source-integrated microelectronics.

1. Introduction

The fast development of portable and wearable microelectronics has ever-increasingly stimulated the urgent demand for microscale electrochemical energy storage devices with matchable properties, such as flexibility, shape diversity, miniaturization, high safety, environmental adaptation, easy modularization, and integration.[1–6] Micro-supercapacitors (MSCs) have been regarded as a very promising class of microscale energy storage devices due to ultrahigh power density, ultrafast charge–discharge rate, exceptional cycling stability, and remarkable safety, which can either complement lithium thin-film batteries or serve as stand-alone microscale power sources.[7,8] However, conventional MSCs with sandwich-like stacked geometry are limited by bulk volume, fixed shape, poor flexibility, and complex integration process, thereby hardly satisfying stringent requirement of future microelectronics.[9] Recently, planar MSCs, enabled by two electrodes separated by a narrow physical interspace on one single substrate, have attracted considerable attention because they are highly advantageous for engineering integrated MSCs with tailored voltage and current output through facile serial and parallel interconnection, and simultaneously possess various form factors of remarkable flexibility and high integrity of modular energy storage pack.[10,11]

So far, great advances of planar MSCs have been achieved in the development of nanostructured active materials. In particular, graphene,[12–14] and its analogous 2D nanosheets,[15] including MXene,[16,17] phosphorene,[18] metal oxides (e.g., MnO$_2$),[19] conducting polymers (e.g., polyaniline,

X. Y. Shi, Prof. X. H. Bao
Department of Chemical Physics
University of Science and Technology of China
96 Jinzhai Road, Hefei 230026, China
X. Y. Shi, Dr. F. Zhou, Prof. Z.-S. Wu, Prof. X. H. Bao
Dalian National Laboratory for Clean Energy
Dalian Institute of Chemical Physics
Chinese Academy of Sciences (CAS)
457 Zhongshan Road, Dalian 116023, China
E-mail: wuzs@dicp.ac.cn

The ORCID identification number(s) for the author(s) of this article can be found under https://doi.org/10.1002/adfm.201902860.

DOI: 10.1002/adfm.201902860

X. Y. Shi, Prof. X. H. Bao
State Key Laboratory of Catalysis
Dalian Institute of Chemical Physics
Chinese Academy of Sciences
457 Zhongshan Road, Dalian 116023, China
J. X. Peng, Prof. R. A. Wu
Laboratory of High-Resolution Mass Spectrometry Technologies
CAS Key Laboratory of Separation Science for Analytical Chemistry
Dalian Institute of Chemical Physics
Chinese Academy of Sciences
457 Zhongshan Road, Dalian 116023, China
J. X. Peng
University of Chinese Academy of Sciences
19 A Yuquan Rd, Shijingshan District, Beijing 100049, China

polypyrrole),[20,21] with ultrathin 2D structure, large surface area, abundant active sites, and remarkable flexibility, are rising as an emerging class of high-performance electrode platform for the construction of planar MSCs in which the electrolyte ions could rapidly diffuse and transfer alone the planes of 2D nanosheets to ultimately boost rate capability and power density.[22] Moreover, various microfabrication strategies, including photolithography,[23–26] printing technologies (e.g., spray coating,[10,27] inkjet printing,[28,29] screen printing,[30,31] 3D printing[32]), mask-assisted filtration,[18] photochemical reduction,[33] laser scribing,[34–38] and electrodeposition,[39] have been developed to construct planar MSCs, tremendously improving the functionality and electrochemical performance of MSCs. However, the synthesis of 2D nanosheets (e.g., graphene) and subsequent fabrication of patterning microelectrodes are generally involved in multistep complex processes, both of which are normally separated, resulting in great challenges unsolved in low-cost, rapid, scalable one-step fabrication and fast integration of high-performance MSCs simultaneously. To overcome this issue, Tour's group developed a one-step, scalable laser scribing technique for directly producing and patterning 3D porous graphene films derived from photothermal conversion of commercial polymers.[40] The resulting laser-induced graphene (LIG) exhibited high electrical conductivity (25 S cm^{-1}), and can be readily patterned to interdigital microelectrodes for planar MSCs. Using this technique, a series of LIG-based materials, e.g., boron-doped LIG,[41] metal oxide/LIG composites,[42] hydrophilic and hydrophobic LIG,[43] have been explored for potential applications in polymer-written electronics, sensors and energy storage devices.[36,44–48] Despite of great progress of LIG as microelectrodes for single cell, one-step scalable fabrication of highly integrated LIG-based MSCs with alterable shape and high-temperature performance has not been yet achieved.

Herein, we demonstrated one-step, cost-effective, and scalable production of LIG micropatterns for highly integrated MSCs (denoted as LIG-MSCs), free of metal current collectors, interconnects, and extra substrate, through laser scribing commercial polyimide (PI) membrane for simultaneous fabrication and patterning of LIG films. The produced LIG films are consisting of randomly stacked graphene nanosheets, and display 3D interconnected porous network, large surface area (≈203 m^2 g^{-1}), and high electrical conductivity (≈8.5 S cm^{-1}). Moreover, the resulting all-solid-state LIG-MSCs not only exhibited favorable electrochemical performance, shape and size diversity, outstanding flexibility, but also represented the fast modularization feature of producing highly integrated LIG-MSCs with adjustable voltage and current output, through customized serial and parallel arrangement of tens to hundreds of individual cells, indicative of great potential as on-chip power sources for miniaturized electronics. Remarkably, our LIG-MSCs working in ionic liquid electrolyte could operate stably at a high temperature of 100 °C for a significant long time, demonstrative of exceptional safety reliability and wide applicability.

2. Results and Discussion

The laser scribing fabrication of LIG-MSCs is schematically illustrated in **Figure 1**a. First, using a computer-controlled blue-violet laser, the PI films were one-step photothermally converted and directly patterned to form the LIG microelectrodes with various in-plane geometries, e.g., interdigital, concentric circular, linear, and foldable shapes (Figure 1b–e). Subsequently, a polymer gel electrolyte of polyvinyl alcohol/H_3PO_4 (PVA/H_3PO_4) or ionogel electrolyte of 1-butyl-3-methylimidazolium hexafluorophosphate and poly(vinylidene difluoride-*co*-hexafluoropropylene) (BMIMPF$_6$-PVDF-HFP), serving as electrolyte, was slowly drop-casted onto the localized microelectrode area and solidified for 12 h. Finally, the all-solid-state LIG-MSCs were readily constructed.

The color changed from light orange to dark (Figure 1b–e), indicative of the efficient conversion of PI into LIG films. Top-view and cross-section scanning electron microscope (SEM) images depicted the successful formation of 3D porous network structure composed of ultrathin randomly stacked graphene nanosheets (Figure 1f,g). Transmission electron microscope (TEM) and high-resolution TEM (HRTEM) (Figure 1h,i; Figure S1, Supporting Information) of LIG showed ultrathin and flat morphology, large lateral size of several micrometers, and a few number of graphitic layers observed from the edges of graphene, manifesting high-quality of LIG. This result was also demonstrated by comparing Fourier-transform infrared spectra (FTIR) and Raman characterizations of LIG with PI films, in which, after laser irradiation of PI, the absence of absorption peaks from 600 to 1700 cm^{-1} in LIG (Figure 1j) and the new appearances of D peak at 1345 cm^{-1}, G peak at 1577 cm^{-1}, and 2D peak at 2684 cm^{-1} as well as high G/D intensity ratio (≈1.4) in LIG (Figure 1k) revealed the formation of high-degree graphene layers. Further, X-ray diffraction (XRD) pattern exhibited high crystallinity, with a typical interlayer spacing of 3.4 Å ($2\theta = 25.9°$) (Figure 1l), and X-ray photoelectron spectroscopy (XPS) confirmed the domination of C—C peak, and high content of C element (>90%) of LIG (Figure 1m). Moreover, high electrical conductivity (≈8.5 S cm^{-1}) and specific surface area (≈203 m^2 g^{-1}) of LIG are greatly beneficial to boost rate performance and capacitance for LIG-MSCs.

To demonstrate the outstanding performance, we first examined single cell of interdigital LIG-MSCs as a typical example in PVA/H_3PO_4 gel electrolyte (**Figure 2**a), carrying out cyclic voltammetry (CV) tests at scan rates from 5 to 2000 mV s^{-1} (Figure 2b,c), galvanostatic charge-discharge (GCD) tests at current densities from 0.01 to 0.1 mA cm^{-2} (Figure 2d) and electrochemical impedance spectroscopy (EIS, Figure 2f). It is clearly seen that the CV curves exhibited nearly rectangle shapes even at a high scan rate of 2000 mV s^{-1}, and GCD profiles showed almost symmetric triangle shapes and negligible voltage drop, indicative of ideal electric double layer capacitive behaviors. Notably, LIG-MSCs disclosed an impressive areal capacitance of 0.62 mF cm^{-2} at 5 mV s^{-1}, which is comparable to the recently reported carbon-based MSCs, such as lithographically patterned activated carbon (0.03 mF cm^{-2}),[49] laser written graphene (0.51 mF cm^{-2}),[50] photoreduced graphene (0.53 mF cm^{-2})[33] and methane plasma reduced graphene (MPG, 0.08 mF cm^{-2}),[23] lithographically patterned graphene (0.12 mF cm^{-2}),[24] spray coated graphene-PH1000 (0.87 mF cm^{-2}),[51] inkjet-printed graphene (0.7 mF cm^{-2}),[29] screen-printed graphene (1.0 mF cm^{-2}),[31] and mask-assisted filtrated graphene-phosphorene (9.8 mF cm^{-2}).[18] It is worth

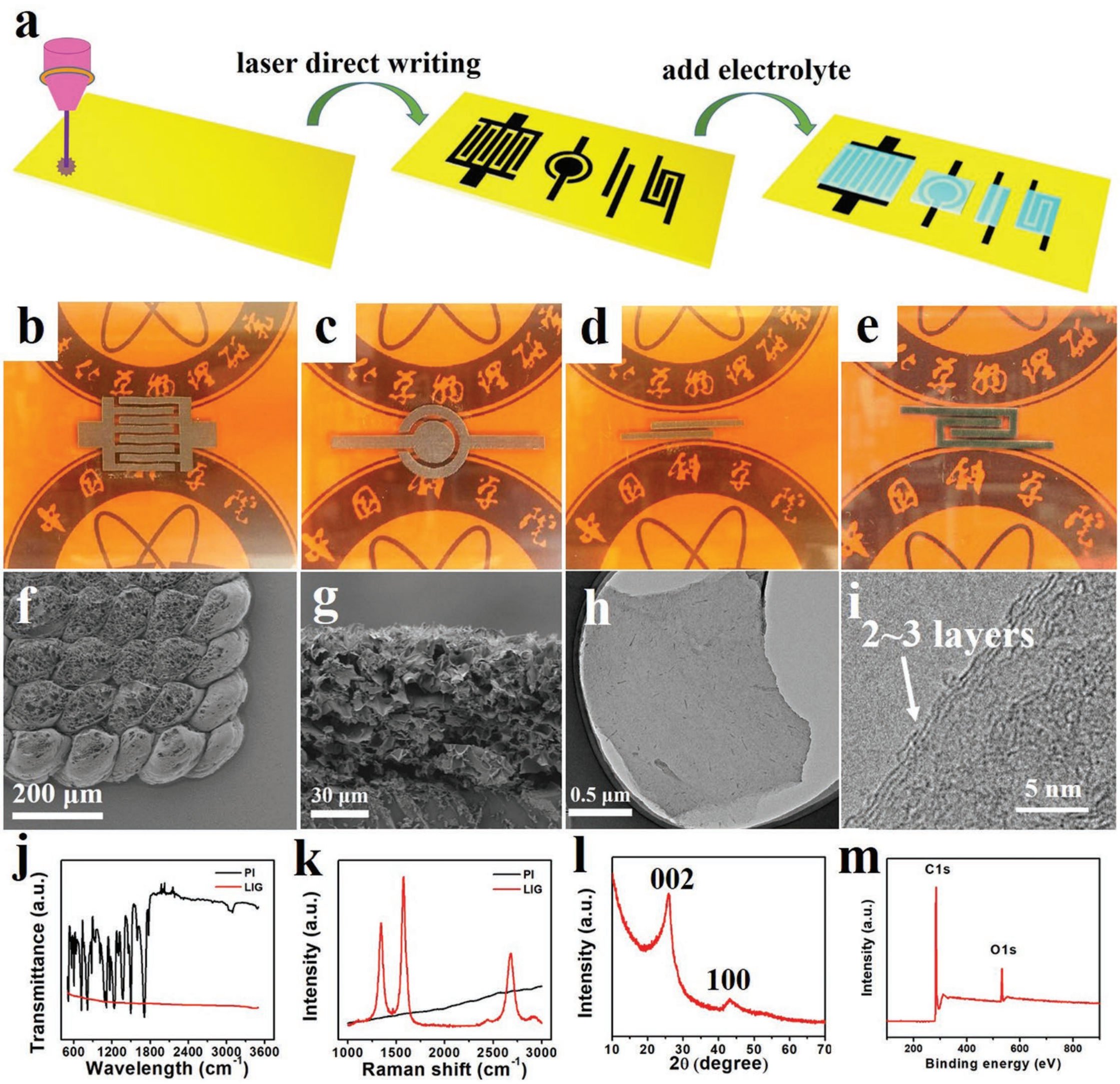

Figure 1. Fabrication and characterization of LIG films for MSCs. a) Fabrication illustration of LIG-MSCs with diverse in-plane geometries. Photographs of LIG-MSCs with in-plane geometries of b) interdigital, c) concentric circular, d) linear, and e) foldable shapes. f) Top-view and g) cross-section SEM images of LIG films, with a thickness of ≈82 µm. h) TEM and i) HRTEM images of LIG. j) FTIR and k) Raman spectra of LIG and PI films. l) XRD pattern and m) XPS spectrum of LIG.

noting that areal capacitance can be further enhanced by addition of redox species (e.g., benzoquinone-hydroquinone) into electrolyte,[52] deposition of high-pseudocapacitance materials (e.g., metal oxides, conducting polymers), construction of asymmetric MSCs,[53] and utilization of heteroatom doping.[41] As demonstrated, areal capacitance of LIG-MSCs was largely increased to 16.3 mF cm^{-2} through electrodeposition of high-pseudocapacitance MnO_2 on LIG microelectrodes (Figure S2, Supporting Information). Further, a high capacitance of 0.40 mF cm^{-2} was retained even at a high scan rate of 500 mV s^{-1} (64.5% of the value at 5 mV s^{-1}), indicating remarkable rate capability of our LIG-MSCs. Moreover, our LIG-MSCs showed excellent electrochemical stability after long cycles of 10 000 times (Figure 2e), during which the slight increase of capacitance (≈3%) possibly resulted from increasing accessible active sites with charge-discharge processes. This excellent performance of LIG-MSCs was further confirmed by EIS plot, which elucidated a nearly vertical line at low frequency (Figure 2f), and a low equivalent series resistance and charge transfer resistance of ≈91 and ≈5 Ω, respectively, manifesting remarkable electric double layer capacitive behavior and fast ionic diffusion. Besides exceptional electrochemical performances, our LIG-MSCs also exhibited impressive mechanical flexibility. It is disclosed that both CV and GCD curves tested in different bent states from 0 to 180° kept well overlapped (Figure 2g,h; Figure S3, Supporting Information), suggesting high robust stability of LIG-MSCs.

To highlight shape diversity of our microdevices, we constructed four designable-shaped LIG-MSCs, with interdigital, concentric circular, linear and foldable planar geometries, the size parameters of which are shown in Figure S4 (Supporting Information), and compared their electrochemical performance. Apparently, all these four LIG-MSCs displayed similar CV curves (**Figure 3**a; Figures S5–S7, Supporting Information)

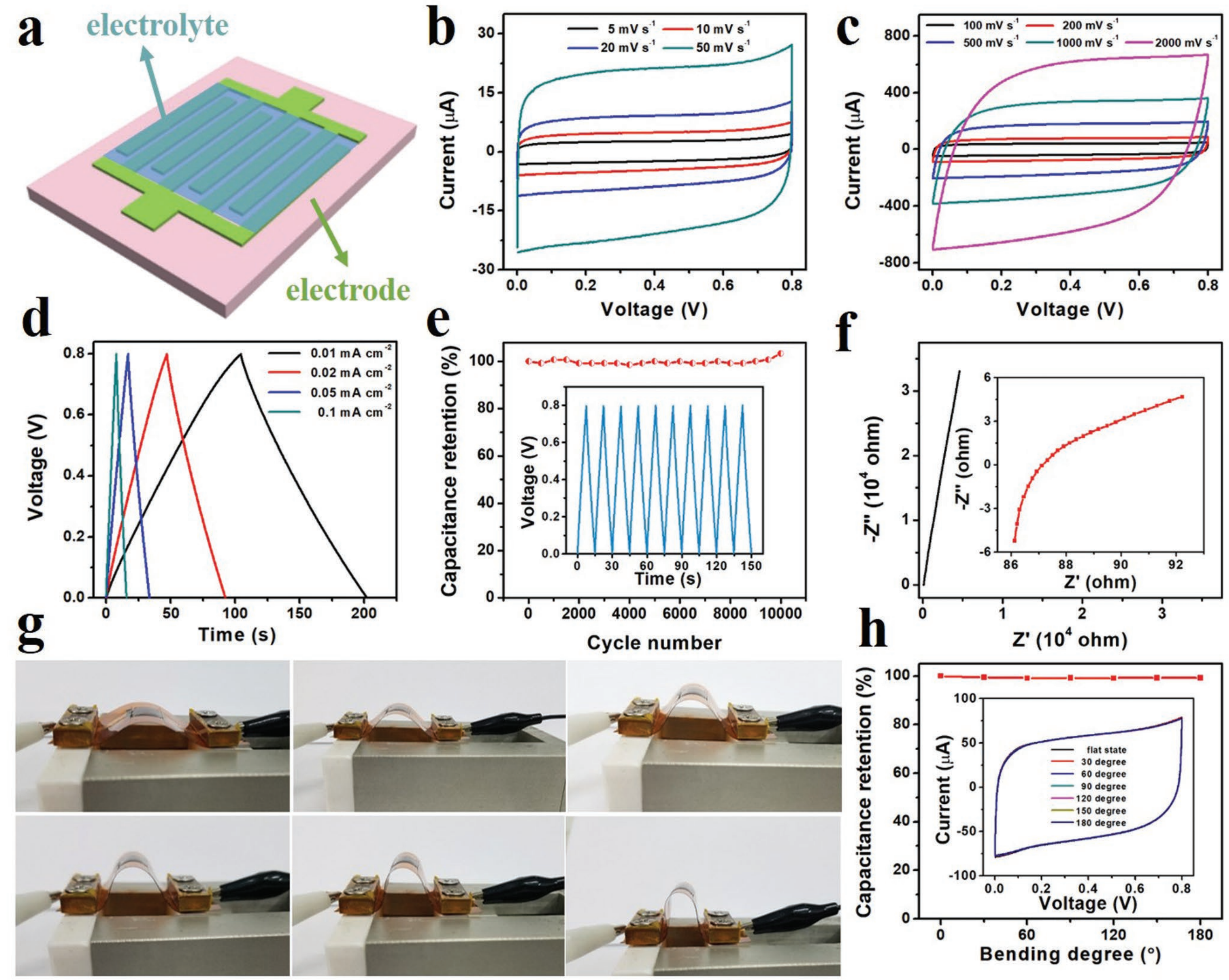

Figure 2. Electrochemical characterization and mechanical flexibility of LIG-MSCs with interdigital geometry in PVA/H_3PO_4 electrolyte. a) Schematic diagram of interdigital LIG-MSCs. b,c) CV curves of LIG-MSCs obtained at scan rates of 5–2000 mV s^{-1}. d) GCD profiles of LIG-MSCs tested at current densities of 0.01–0.1 mA cm^{-2}. e) Cycling stability of LIG-MSCs for 10 000 cycles, tested at 0.11 mA cm^{-2}. Inset is the GCD profiles during cycles. f) Complex plane plot of LIG-MSCs. Inset: a magnified curve in high-frequency region. g) Photographs of LIG-MSCs with interdigital geometry in different bent states. h) Capacitance retention of LIG-MSCs under different bent states compared to the value in flat state. Inset: CV curves obtained at 100 mV s^{-1}.

and areal capacitance of 0.55–0.73 mF cm^{-2} at a low scan rate of 20 mV s^{-1} (Figure 3b), demonstrative of outstanding shape diversity and applicability. However, the disparity of rate performance was observed, both of interdigital and linear shaped LIG-MSCs displayed better rate capability, showing an initial capacitance retention of 73% and 70% at 500 mV s^{-1}, higher than those of concentric circular (59%) and foldable (41%) planar geometries (Figure 3c). It is indicated that the elaborated design and systematical optimization of device geometry are highly necessary to maximize the performance. In addition, tandem LIG-MSCs with concentric circular and foldable shapes (Figure 3d,g), making use of LIG patterns simultaneously acting as microelectrodes and conducting interconnects, free of metal-based current collectors and connects, exhibited ideal tandem capacitive behaviors, from the increased output voltage and almost unchanged charge/discharge time as serial cell number (Figure 3e,f,h,i; Figures S8 and S9, Supporting Information), further suggestive of shape diversity and favorable integration of our LIG-MSCs.

To further demonstrate outstanding integration and performance uniformity of our technique, we constructed energy storage modular packs of highly integrated LIG-MSCs (xS × yP, x and y represent the number of cells connected in series and in parallel), consisting of multiple cells connected in series and/or in parallel (**Figure 4**a–d). As proof of concept, the linear tandem integrated LIG-MSCs (xS × 1P, x = 1–10) connected in an in-series fashion from 1 to 10 cells could stably output the stepwise increased voltage from 0.8 to 8 V, as demonstrated in CV and GCD results (Figure 4e–g, Figure S10, Supporting Information). Such ideal tandem capacitive behaviors of LIG-MSCs (xS × 1P, x = 1–10) were also demonstrated by monotonic capacitance decline (Figure 4f) and nearly invariable charge/discharge time (Figure 4g, Figure S10, Supporting Information). Furthermore, the total current output of integrated LIG-MSCs (1S × yP,

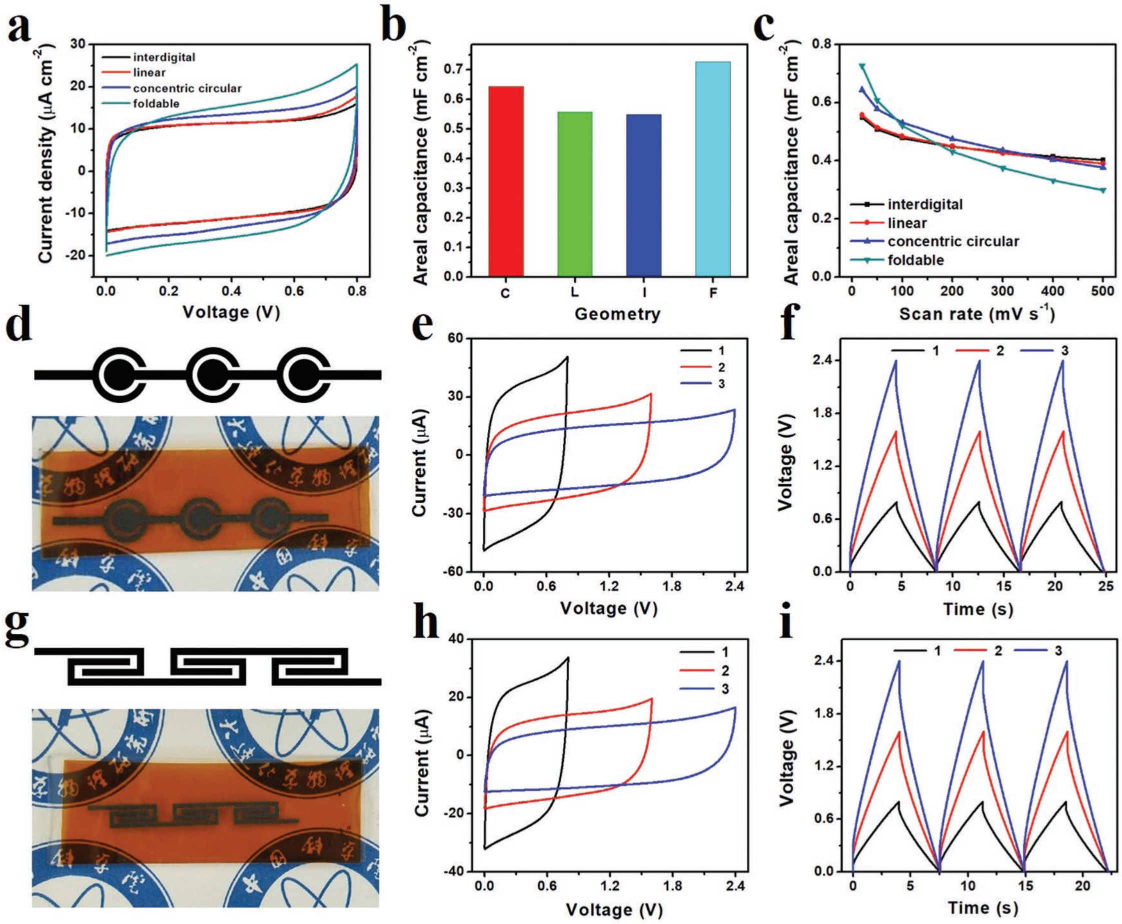

Figure 3. Shape diversity of LIG-MSCs. a) CV curves of LIG-MSCs with different in-plane geometries obtained at a scan rate of 20 mV s^{-1}. b) Areal capacitance of LIG-MSCs with various shapes (C: concentric circular, L: linear, I: interdigital, F: foldable) obtained at a scan rate of 20 mV s^{-1}. c) Areal capacitance of designable-shaped LIG-MSCs as a function of scan rate. d) Diagram and digital image of tandem LIG-MSCs with concentric circular geometry. e) CV curves tested at a scan rate of 100 mV s^{-1} with different serial number. f) GCD profiles tested at 64 μA with different serial number. g) Diagram and digital image of tandem LIG-MSCs with foldable geometry. h) CV curves tested at a scan rate of 100 mV s^{-1} with different serial number. i) GCD profiles tested at 44 μA with different serial number.

y = 1–4) was also proportionally improved by increasing the number of the connected cells in parallel while the voltage kept unchanged (Figure S11, Supporting Information). More importantly, our integrated LIG-MSCs with complex connection (4S × yP, y = 1–4) disclosed a stable high voltage of 3.2 V and stepwise enhanced capacitance from 4S × 1P to 4S × 4P (Figure 4h–j, Figure S12, Supporting Information), suggestive of exceptional performance uniformity. This result further validated the output voltage and current of our modular LIG-MSCs could be readily adjustable in term of the requirements of actual applications, indicative of favorable customization of our technique. Besides, linear-shaped integrated LIG-MSCs (3S × 1P) exhibited remarkable flexibility, as demonstrated by nearly coincident CV curves tested in different bent states (Figure S13, Supporting Information). More importantly, our integrated LIG-MSCs (3S × 1P) can directly serve as standalone microscale power sources to power a liquid crystal display (LCD, Figure 4d), showing the logo of "Dalian Institute of Chemical Physics." Therefore, our technique is highly flexible for one-step, cost-effective, scalable production of integrated energy storage packs with adjustable performance to fulfill the requirements in actual microelectronics.

Besides high performance and superior integration, future MSCs are highly required to be operated stably and durably at high temperature (>60 °C) for special occasions, e.g., oil drilling, military and aero environments.[54,55] However, most reported MSCs can't work stably over 60 °C due to low boiling point of the used solvents (e.g., water, acetonitrile), inflammability of organic electrolytes, and poor thermal endurance of separators.[55–57] To this regard, combining the advantage of intrinsically high thermal stability of PI (>200 °C) and ionic liquid (≈150 °C),[5,6,58] LIG microelectrodes produced through a high-temperature photothermal process (>2000 °C),[36,40] and advanced separator-free in-plane device geometry, we fabricated all-solid-state LIG-MSCs (denoted as LIG-MSCs-IL) using high-temperature stable ionogel electrolyte of BMIMPF$_6$-PVDF-HFP. As expected, our LIG-MSCs-IL could operate stably at a wide range of temperature from 25, 50 to 75 and 100 °C (Figures S14–S16, Supporting Information; **Figure 5**), and nearly rectangle CV curves and symmetric triangular GCD

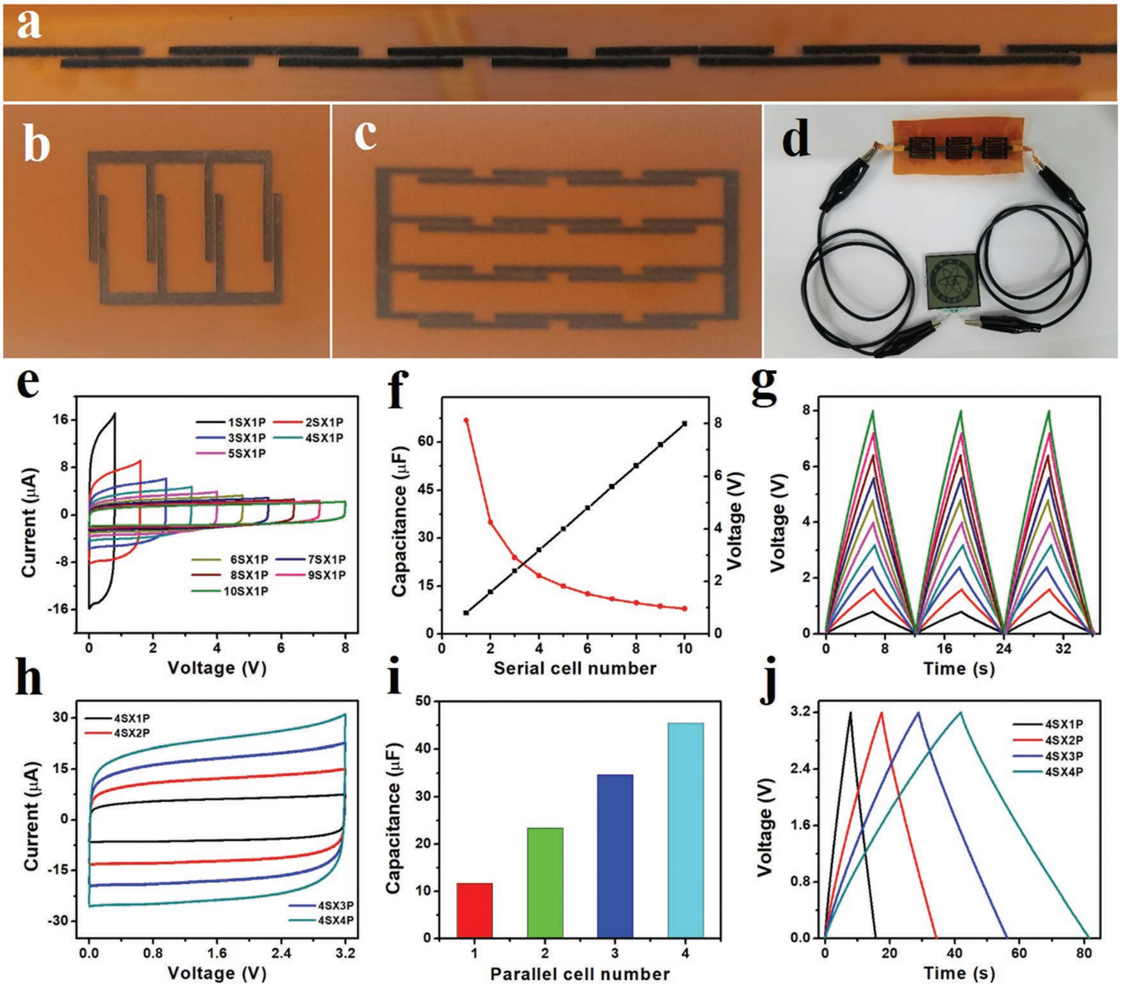

Figure 4. Integration and performance uniformity of LIG-MSCs. Photographs of integrated LIG-MSCs with linear-shape in-plane geometry connected in various arrangements of a) 10S × 1P, b) 1S × 4P, and c) 4S × 4P. d) Photograph of three serially connected LIG-MSCs with interdigital in-plane geometry for powering an LCD. e) CV curves of integrated LIG-MSCs with different serial number (1, 2, 3, ..., 10S × 1P) obtained at a scan rate of 200 mV s^{-1}. f) Capacitance and voltage output of LIG-MSCs as functions of serial cell number (1, 2, 3, ..., 10S × 1P). g) GCD profiles of LIG-MSCs (1, 2, 3, ..., 10S × 1P) measured at 10 μA. h) CV curves, i) capacitance obtained at a scan rate of 500 mV s^{-1}, and j) GCD profiles tested at 5 μA of integrated LIG-MSCs connected in a serial and a parallel fashion from 4S × 1P to 4S × 4P.

profiles were observed even at 100 °C (Figure 5a,b,d), indicative of high-temperature stability. Moreover, it is worth noting that areal capacitance of LIG-MSCs-IL, tested at 5 mV s^{-1}, was gradually improved from ≈0.8 mF cm^{-2} at 25 °C to ≈1.7 mF cm^{-2} at 100 °C with increasing temperature (Figure 5c; Figures S14–S17, Supporting Information), possibly due to enhanced ionic conductivity of ionogel electrolyte at high temperature.[11,58] Notably, our LIG-MSCs-IL exhibited long-term cycling stability at 100 °C (Figure 5e), with ≈90% capacitance retention after 3000 cycles, suggestive of tremendous availability of ionogel-based LIG-MSCs in high-temperature environments. The Ragone plot (Figure 5f) compared areal energy density and power density of LIG-MSCs tested in PVA/H_3PO_4 aqueous electrolyte (denoted as LIG-MSCs-AE) and BMIMPF$_6$-PVDF-HFP at 25 °C (LIG-MSCs-IL-25) and 100 °C (LIG-MSCs-IL-100), and some state-of-the-art MSCs. Remarkably, our LIG-MSCs-IL-100 disclosed an impressive areal energy density of ≈0.92 μWh cm^{-2}, much higher than LIG-MSCs-IL-25 (≈0.47 μWh cm^{-2}) and graphene fiber@3D graphene (GF@3D-G-MSC, ≈0.16 μWh cm^{-2}),[59] and one order of magnitude higher than LIG-MSCs-AE (≈0.06 μWh cm^{-2}), MPG-MSCs (≈0.04 μWh cm^{-2}),[23] and photolithographic MSCs with 32 fingers (P-MSCs-32, ≈0.06 μWh cm^{-2}),[24] indicative of tremendous potential of our LIG-MSCs as stand-alone power sources for miniaturized electronics.

The outstanding performance of LIG-MSCs was mainly attributed to the one-step realization of producing PI-derived high-quality LIG, engineering LIG microelectrodes and metal-free interconnects into the separator-free planar geometry of integrated MSCs. Specifically, i) LIG microelectrodes possess 3D interconnected porous network of randomly stacked graphene nanosheets, large accessible surface area, and high electrical conductivity, which can ensure fast ionic diffusion and rapid electron transport, resulting in high energy density and power density. ii) Elaborated design of in-plane device geometry, intrinsic flexibility of PI substrates, exceptional mechanical properties of LIG nanosheets and usage of solid-state electrolyte led to

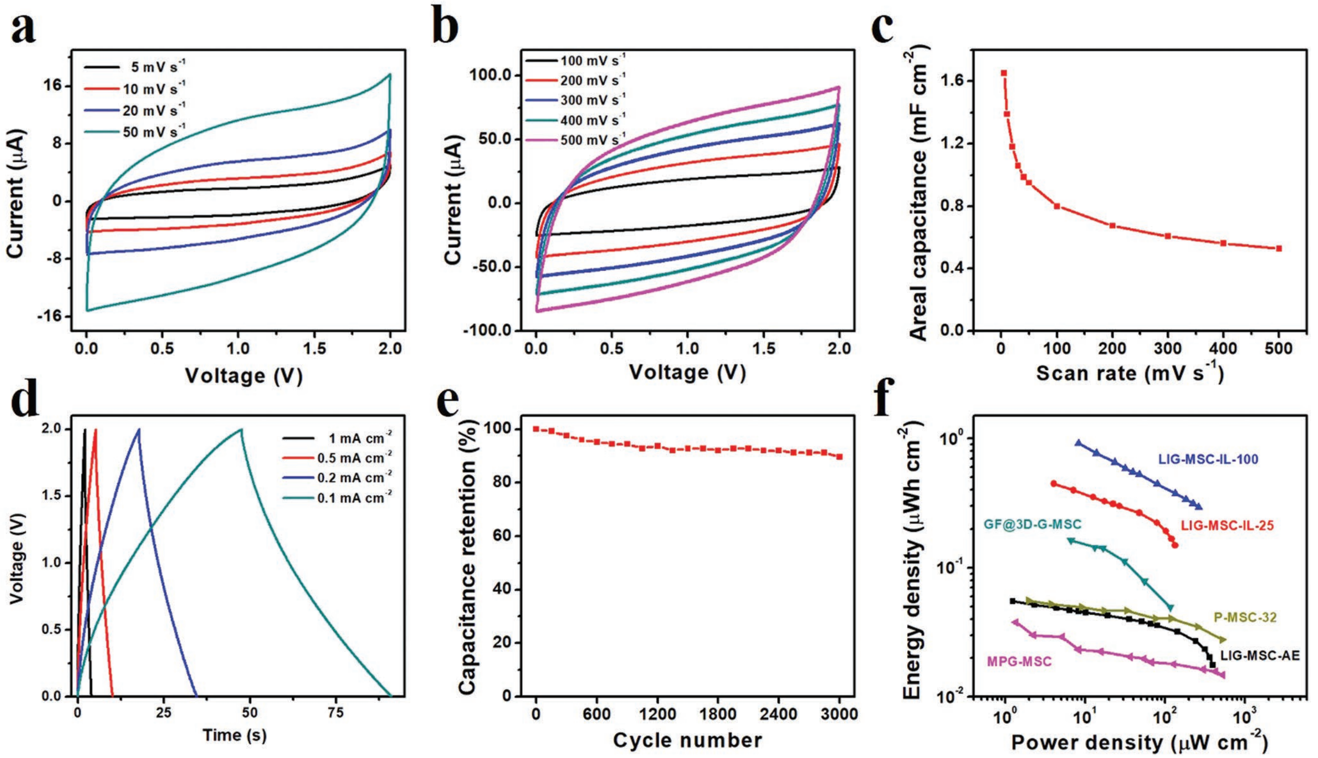

Figure 5. High-temperature performance of linear-shape LIG-MSCs tested in ionogel electrolyte of BMIMPF$_6$-PVDF-HFP at 100 °C. a,b) CV curves of LIG-MSCs obtained at scan rates from 5 to 500 mV s^{-1}. c) Areal capacitance of LIG-MSCs as a function of scan rate. d) GCD profiles of LIG-MSCs tested at current densities of 0.1–1 mA cm^{-2}. e) Cycling stability of LIG-MSCs for 3000 cycles, tested at a current density of 0.4 mA cm^{-2}. f) Ragone plot of LIG-MSCs-AE, LIG-MSCs-IL-25, LIG-MSCs-IL-100, and some state-of-the-art MSCs.

remarkable flexibility of LIG-MSCs. iii) The resulting LIG-MSCs exhibited favorable shape diversity and designability, providing great opportunities to realize delicate and artistic MSC patterns, for applications in wearable and portable electronics. iv) The PI-derived high-conducting LIG patterns, strongly bonded on PI substrate, can not only serve as binder-free flexible microelectrodes, but also act as metal-free current collectors and interconnects, endowing ultrahigh integrity, superior modularization and performance uniformity of integrated MSCs. v) Combination of excellent thermal stability of BMIMPF$_6$-PVDF-HFP ionogel electrolyte and PI substrates, along with advanced separator-free planar geometry, guaranteed remarkable high-temperature performance durability of LIG-MSCs, all of which could not be obtained by conventional strategies.[23,50,60,61]

3. Conclusion

In summary, we demonstrated rapid, cost-effective, and scalable fabrication of all-solid-state highly integrated LIG-MSCs with various intriguing features of exceptional shape diversity, outstanding flexibility, excellent performance uniformity, superior integration, and high-temperature stability. The one-step realization of active material preparation, patterning of microelectrodes, and serial/parallel integration significantly simplify the whole fabrication process, endowing ultrahigh integrity, exceptional flexibility, and tailored voltage and capacitance output, and our technique is readily extended to fabrication of hundreds and thousands of MSCs, holding enormous potential in performance-customized microelectronics and integrated circuits. More importantly, through elaborate design and combination of intrinsic thermal stability of PI substrates, separator-free planar device geometry, and high-temperature stable ionic liquid electrolyte, LIG-MSCs-IL displayed excellent high-temperature performance, indicative of broad applicability. Therefore, we believe that our LIG-MSCs represent impressive opportunities as standalone microscale power sources in various applications including but not limited to flexible and wearable microelectronics, biomedical devices, oil drilling, military and aerospace fields.

4. Experimental Section

Fabrication of LIG-MSCs: First, the patterned LIG simultaneously acting as microelectrodes, metal-free current collectors, and interconnects was directly fabricated from the one-step photothermal conversion of PI film through a computer-controlled commercial laser (λ = 450 nm) with a maximum power of 2.0 W at a scribing speed of ≈4 mm s^{-1}. With this technique, the LIG microelectrodes with various in-plane geometries, e.g., interdigital, concentric circular, linear, and foldable shapes were manufactured. Subsequently, a polymer gel electrolyte of PVA/H$_3$PO$_4$ or ionogel electrolyte of BMIMPF$_6$-PVDF-HFP was carefully drop-casted onto the localized microelectrode area. After electrolyte solidification and package, the all-solid-state LIG-MSCs were obtained.

For the preparation of PVA/H$_3$PO$_4$ electrolyte, PVA (5 g) and H$_3$PO$_4$ (5 g) in deionized water (50 mL) were mixed at 90 °C for 1 h under stirring. Then it was carefully dropped to cover the area of microelectrodes and solidified in ambient conditions for 12 h.[62]

For the preparation of $BMIMPF_6$-PVDF-HFP electrolyte, $BMIMPF_6$ and PVDF-HFP (mass ratio 9:1) were first dispersed in acetone under stirring. Then, it was dropped to cover the surface of microelectrodes and vacuum dried at 80 °C for 12 h. Afterward, the LIG-MSCs were moved immediately into a glove box.[14]

For the electrodeposition of MnO_2 on LIG microelectrodes, a three-electrode system was used to deposit MnO_2 on LIG microelectrodes by utilizing Ag/AgCl as reference electrode, Pt as counter electrode, LIG as working electrode, in the aqueous electrolyte of 0.1 M $Mn(CH_3COO)_2$ and 0.1 M Na_2SO_4. A constant voltage of 1 V was applied and the mass loading of MnO_2 was controlled by adjusting deposition time from 30 to 90 s. 1 M Na_2SO_4 aqueous solution was selected as electrolyte for the assembly of the symmetric LIG-MnO_2-MSC microdevices.

Materials Characterizations: LIG materials and microelectrodes were characterized by SEM (JEOL JSM-7800F), TEM (JEM-2100), Raman spectroscopy (LabRAM HR 800 Raman spectrometer, 632 nm), FTIR spectrometer (Thermo Fisher Scientific, Nicolet iS50), XRD (X'pert Pro), and XPS (Thermo Fisher, ESCALAB 250xi). Electrical conductivity was tested by a four-point probe resistivity measurement system (RST-9).

Electrochemical Measurements: Electrochemical performance of LIG-MSCs was evaluated by CV measurements at different scan rates from 5 to 2000 mV s^{-1}, GCD profiles conducted at different current densities from 0.01 to 1 mA cm^{-2}, and EIS recorded in the frequency range from 0.01 Hz to 100 kHz with a 5 mV alternating current amplitude, using an electrochemical workstation (CHI 760E). For electrochemical tests of LIG-MSCs-IL at different temperatures of 50, 75, 100 °C, LIG-MSCs-IL were kept in a thermostat box at the target temperature for half an hour before test.

Supporting Information

Supporting Information is available from the Wiley Online Library or from the author.

Acknowledgements

This work was financially supported by the National Key R&D Program of China (Grant 2016YFA0200200), the National Natural Science Foundation of China (Grants 51572259, 51872283, and 21805273), the LiaoNing Revitalization Talents Program (Grant XLYC1807153), the Natural Science Foundation of Liaoning Province (Grant 20180510038), the Dalian National Laboratory For Clean Energy (DNL), CAS, DICP (Grants DICP ZZBS201708 and DICP ZZBS201802), DICP&QIBEBT (Grant UN201702), the DNL Cooperation Fund, CAS (Grants DNL180310 and DNL180308).

Conflict of Interest

The authors declare no conflict of interest.

Keywords

flexibility, graphene, integrated micro-supercapacitors, performance uniformity, scalable fabrication

Received: April 9, 2019
Revised: August 4, 2019

[1] D. P. Dubal, N. R. Chodankar, D. H. Kim, P. Gomez-Romero, *Chem. Soc. Rev.* **2018**, *47*, 2065.
[2] L. Li, Z. Lou, D. Chen, K. Jiang, W. Han, G. Shen, *Small* **2018**, *14*, 1702829.
[3] L. Wen, F. Li, H.-M. Cheng, *Adv. Mater.* **2016**, *28*, 4306.
[4] W. Liu, M. S. Song, B. Kong, Y. Cui, *Adv. Mater.* **2017**, *29*, 1603436.
[5] S. Zheng, Z.-S. Wu, F. Zhou, X. Wang, J. Ma, C. Liu, Y.-B. He, X. Bao, *Nano Energy* **2018**, *51*, 613.
[6] M. T. F. Rodrigues, G. Babu, H. Gullapalli, K. Kalaga, F. N. Sayed, K. Kato, J. Joyner, P. M. Ajayan, *Nat. Energy* **2017**, *2*, 17108.
[7] L. Liu, Z. Niu, J. Chen, *Chem. Soc. Rev.* **2016**, *45*, 4340.
[8] N. A. Kyeremateng, T. Brousse, D. Pech, *Nat. Nanotechnol.* **2017**, *12*, 7.
[9] D. Qi, Y. Liu, Z. Liu, L. Zhang, X. Chen, *Adv. Mater.* **2017**, *29*, 1602802.
[10] X. Shi, Z.-S. Wu, J. Qin, S. Zheng, S. Wang, F. Zhou, C. Sun, X. Bao, *Adv. Mater.* **2017**, *29*, 1703034.
[11] S. Zheng, J. Ma, Z.-S. Wu, F. Zhou, Y.-B. He, F. Kang, H.-M. Cheng, X. Bao, *Energy Environ. Sci.* **2018**, *11*, 2001.
[12] X. Shi, S. Zheng, Z.-S. Wu, X. Bao, *J. Energy Chem.* **2018**, *27*, 25.
[13] Z.-S. Wu, Y. Z. Tan, S. Zheng, S. Wang, K. Parvez, J. Qin, X. Shi, C. Sun, X. Bao, X. Feng, K. Müllen, *J. Am. Chem. Soc.* **2017**, *139*, 4506.
[14] F. Zhou, H. Huang, C. Xiao, S. Zheng, X. Shi, J. Qin, Q. Fu, X. Bao, X. Feng, K. Müllen, Z.-S. Wu, *J. Am. Chem. Soc.* **2018**, *140*, 8198.
[15] P. Zhang, F. Wang, M. Yu, X. Zhuang, X. Feng, *Chem. Soc. Rev.* **2018**, *47*, 7426.
[16] Y.-Y. Peng, B. Akuzum, N. Kurra, M.-Q. Zhao, M. Alhabeb, B. Anasori, E. C. Kumbur, H. N. Alshareef, M.-D. Ger, Y. Gogotsi, *Energy Environ. Sci.* **2016**, *9*, 2847.
[17] C. J. Zhang, M. P. Kremer, A. Seral-Ascaso, S.-H. Park, N. McEvoy, B. Anasori, Y. Gogotsi, V. Nicolosi, *Adv. Funct. Mater.* **2018**, *28*, 1705506.
[18] H. Xiao, Z.-S. Wu, L. Chen, F. Zhou, S. Zheng, W. Ren, H.-M. Cheng, X. Bao, *ACS Nano* **2017**, *11*, 7284.
[19] M. F. El-Kady, M. Ihns, M. Li, J. Y. Hwang, M. F. Mousavi, L. Chaney, A. T. Lech, R. B. Kaner, *Proc. Natl. Acad. Sci. USA* **2015**, *112*, 4233.
[20] J. Qin, F. Zhou, H. Xiao, R. Ren, Z.-S. Wu, *Sci. China Mater.* **2018**, *61*, 233.
[21] C. Gao, J. Gao, C. Shao, Y. Xiao, Y. Zhao, L. Qu, *J. Mater. Chem. A* **2018**, *6*, 19750.
[22] J. J. Yoo, K. Balakrishnan, J. Huang, V. Meunier, B. G. Sumpter, A. Srivastava, M. Conway, A. L. Reddy, J. Yu, R. Vajtai, P. M. Ajayan, *Nano Lett.* **2011**, *11*, 1423.
[23] Z.-S. Wu, K. Parvez, X. Feng, K. Müllen, *Nat. Commun.* **2013**, *4*, 2487.
[24] Z.-S. Wu, K. Parvez, X. Feng, K. Müllen, *J. Mater. Chem. A* **2014**, *2*, 8288.
[25] T. M. Dinh, K. Armstrong, D. Guay, D. Pech, *J. Mater. Chem. A* **2014**, *2*, 7170.
[26] K. U. Laszczyk, K. Kobashi, S. Sakurai, A. Sekiguchi, D. N. Futaba, T. Yamada, K. Hata, *Adv. Energy Mater.* **2015**, *5*, 1500741.
[27] Z. Liu, Z.-S. Wu, S. Yang, R. Dong, X. Feng, K. Müllen, *Adv. Mater.* **2016**, *28*, 2217.
[28] K.-H. Choi, J. Yoo, C. K. Lee, S.-Y. Lee, *Energy Environ. Sci.* **2016**, *9*, 2812.
[29] J. Li, S. Sollami Delekta, P. Zhang, S. Yang, M. R. Lohe, X. Zhuang, X. Feng, M. Östling, *ACS Nano* **2017**, *11*, 8249.
[30] S. Xu, Y. Dall'Agnese, G. Wei, C. Zhang, Y. Gogotsi, W. Han, *Nano Energy* **2018**, *50*, 479.
[31] X. Shi, S. Pei, F. Zhou, W. Ren, H.-M. Cheng, Z.-S. Wu, X. Bao, *Energy Environ. Sci.* **2019**, *12*, 1534.
[32] V. G. Rocha, E. Garcia-Tunon, C. Botas, F. Markoulidis, E. Feilden, E. D'Elia, N. Ni, M. Shaffer, E. Saiz, *ACS Appl. Mater. Interfaces* **2017**, *9*, 37136.
[33] S. Wang, Z.-S. Wu, S. Zheng, F. Zhou, C. Sun, H.-M. Cheng, X. Bao, *ACS Nano* **2017**, *11*, 4283.
[34] M. F. El-Kady, R. B. Kaner, *Nat. Commun.* **2013**, *4*, 1475.

[35] J. Ye, H. Tan, S. Wu, K. Ni, F. Pan, J. Liu, Z. Tao, Y. Qu, H. Ji, P. Simon, Y. Zhu, *Adv. Mater.* **2018**, *30*, 1801384.

[36] X. Li, W. Cai, K. S. Teh, M. Qi, X. Zang, X. Ding, Y. Cui, Y. Xie, Y. Wu, H. Ma, Z. Zhou, Q. A. Huang, J. Ye, L. Lin, *ACS Appl. Mater. Interfaces* **2018**, *10*, 26357.

[37] J. Gao, C. Shao, S. Shao, F. Wan, C. Gao, Y. Zhao, L. Jiang, L. Qu, *Small* **2018**, *14*, 1801809.

[38] G. Sun, H. Yang, G. Zhang, J. Gao, X. Jin, Y. Zhao, L. Jiang, L. Qu, *Energy Environ. Sci.* **2018**, *11*, 3367.

[39] R. Guo, J. Chen, B. Yang, L. Liu, L. Su, B. Shen, X. Yan, *Adv. Funct. Mater.* **2017**, *27*, 1702394.

[40] J. Lin, Z. Peng, Y. Liu, F. Ruiz-Zepeda, R. Ye, E. L. Samuel, M. J. Yacaman, B. I. Yakobson, J. M. Tour, *Nat. Commun.* **2014**, *5*, 5714.

[41] Z. Peng, R. Ye, J. A. Mann, D. Zakhidov, Y. Li, P. R. Smalley, J. Lin, J. M. Tour, *ACS Nano* **2015**, *9*, 5868.

[42] R. Ye, Z. Peng, T. Wang, Y. Xu, J. Zhang, Y. Li, L. G. Nilewski, J. Lin, J. M. Tour, *ACS Nano* **2015**, *9*, 9244.

[43] Y. Li, D. X. Luong, J. Zhang, Y. R. Tarkunde, C. Kittrell, F. Sargunaraj, Y. Ji, C. J. Arnusch, J. M. Tour, *Adv. Mater.* **2017**, *29*, 1700496.

[44] R. Ye, D. K. James, J. M. Tour, *Acc. Chem. Res.* **2018**, *51*, 1609.

[45] L. Q. Tao, H. Tian, Y. Liu, Z. Y. Ju, Y. Pang, Y. Q. Chen, D. Y. Wang, X. G. Tian, J. C. Yan, N. Q. Deng, Y. Yang, T. L. Ren, *Nat. Commun.* **2017**, *8*, 14579.

[46] J. Cai, C. Lv, A. Watanabe, *Nano Energy* **2016**, *30*, 790.

[47] D. Wu, Q. Peng, S. Wu, G. Wang, L. Deng, H. Tai, L. Wang, Y. Yang, L. Dong, Y. Zhao, J. Zhao, D. Sun, L. Lin, *Sensors* **2018**, *18*, 4405.

[48] J. Cai, C. Lv, A. Watanabe, *J. Mater. Chem. A* **2016**, *4*, 1671.

[49] W. Lu, N. Naoki, Y. Gleb, *ACS Nano* **2013**, *7*, 6498.

[50] W. Gao, N. Singh, L. Song, Z. Liu, A. L. Reddy, L. Ci, R. Vajtai, Q. Zhang, B. Wei, P. M. Ajayan, *Nat. Nanotechnol.* **2011**, *6*, 496.

[51] Z.-S. Wu, Z. Liu, K. Parvez, X. Feng, K. Müllen, *Adv. Mater.* **2015**, *27*, 3669.

[52] D. Vonlanthen, P. Lazarev, K. A. See, F. Wudl, A. J. Heeger, *Adv. Mater.* **2014**, *26*, 5095.

[53] L. Li, J. Zhang, Z. Peng, Y. Li, C. Gao, Y. Ji, R. Ye, N. D. Kim, Q. Zhong, Y. Yang, H. Fei, G. Ruan, J. M. Tour, *Adv. Mater.* **2016**, *28*, 838.

[54] R. S. Borges, A. L. Reddy, M. T. Rodrigues, H. Gullapalli, K. Balakrishnan, G. G. Silva, P. M. Ajayan, *Sci. Rep.* **2013**, *3*, 2572.

[55] B. Qin, X. Wang, D. Sui, T. Zhang, M. Zhang, Z. Sun, Z. Ge, Y. Xie, Y. Zhou, Y. Ren, Y. Han, Y. Ma, Y. Chen, *Energy Technol.* **2018**, *6*, 161.

[56] K. Sung-Kon, K. Hae Jin, L. Jong-Chan, P. V. Braun, P. Ho Seok, *ACS Nano* **2015**, *9*, 8569.

[57] B. Shen, R. Guo, J. Lang, L. Liu, L. Y. Liu, X. Yan, *J. Mater. Chem. A* **2016**, *4*, 8316.

[58] M.-T. F. Rodrigues, K. Kalaga, H. Gullapalli, G. Babu, A. L. M. Reddy, P. M. Ajayan, *Adv. Energy Mater.* **2016**, *6*, 1600218.

[59] Y. Meng, Y. Zhao, C. Hu, H. Cheng, Y. Hu, Z. Zhang, G. Shi, L. Qu, *Adv. Mater.* **2013**, *25*, 2326.

[60] R. Kumar, E. Joanni, R. K. Singh, E. da Silva, R. Savu, L. T. Kubota, S. A. Moshkalev, *J. Colloid Interface Sci.* **2017**, *507*, 271.

[61] Z. Peng, J. Lin, R. Ye, E. L. Samuel, J. M. Tour, *ACS Appl. Mater. Interfaces* **2015**, *7*, 3414.

[62] H. Xiao, Z.-S. Wu, F. Zhou, S. Zheng, D. Sui, Y. Chen, X. Bao, *Energy Storage Mater.* **2018**, *13*, 233.